

Refining the Oort and Galactic constants

Rob P. Olling^{1*}, Michael R. Merrifield^{1†}

¹*Dept. of Physics and Astronomy,
University of Southampton, Southampton SO17 1BJ, U.K.*

Accepted 1998 February 2

ABSTRACT

The local stellar kinematics of the Milky Way offer a useful tool for studying the rotation curve of the Galaxy. These kinematics – usually parameterized by the Oort constants A and B – depend on the local gradient of the rotation curve as well as its absolute value (Θ_0), and the Sun’s distance to the Galactic center (R_0). The density of interstellar gas in the Milky Way is shown to vary non-monotonically with radius, and so contributes significantly to the local gradient of the rotation curve. We have therefore calculated mass models for the Milky Way that include this component, and have derived the corresponding radial variation in the Oort constants. Between $0.9R_0$ and $1.2R_0$ the Oort functions $A(R)$ and $B(R)$ differ significantly from the general $\sim \Theta_0/R$ dependence. Various previously-inexplicable observations are shown to be consistent with these new predictions. For example, these models may explain the $\sim 40\%$ difference between the values for $2AR_0$ derived from radial velocity data originating in the inner and outer Galaxy (Merrifield 1992). They also go some way toward explaining the different shapes of the velocity ellipsoids of giant and dwarf stars in the solar neighbourhood. However, a consistent picture only emerges if one adopts small values for the radius of the solar circle ($R_0 = 7.1 \pm 0.4$ kpc) and local circular speed ($\Theta_0 = 184 \pm 8$ km s⁻¹). With these Galactic constants the Milky Way’s rotation curve declines slowly in the outer Galaxy; $V_{\text{rot}}(20 \text{ kpc}) = 166$ km s⁻¹. Our low value for the distance to the Galactic center agrees well with the only direct determination of R_0 (7.2 ± 0.7 kpc, Reid 1993). Using these Galactic constants, we find that the proper motion of Sgr A* is consistent with the observational constraints (Backer & Sramek 1987; Backer 1996; Reid 1998). Simple analytic arguments as well as detailed calculations show that the radial velocities and proper motions of our best fit model are entirely consistent with the radial velocities of Cepheids (Pont, Mayor & Burki 1994) and the Hipparcos measurements of their proper motions (Feast & Whitelock 1997).

Key words: Galaxy: structure - Galaxy: kinematics and dynamics - Galaxy: solar neighbourhood - Galaxy: fundamental parameters - Galaxy: stellar content - Cepheids - ISM: general

1 INTRODUCTION

Since the first measurements of the Milky Way’s rotation almost seventy years ago, a great deal of effort has been expended in studying its kinematics (e.g., Fich & Tremaine 1991, and references therein). The simplest kinematic quantity that we can determine is the rotation curve, $\Theta(R)$, which

measures the speed of circular orbits as a function of radius. Unfortunately, our location within the Milky Way means that even this simple dynamical quantity is difficult to establish. In particular, the modest uncertainties in our knowledge of the distance to the Galactic center ($R_0 = 7.7 \pm 0.7$ kpc; Reid 1993) and the rotation speed at the solar circle ($\Theta_0 = 200 \pm 20$ km s⁻¹; Sackett 1997) lead to significant uncertainties in the inferred form for $\Theta(R)$ (Fich & Tremaine 1991). Measurements of stellar kinematics provide one approach to constraining the form of the rotation curve. The quantities measured are parameterized by the Oort functions,

* E-mail: olling@astro.soton.ac.uk

† E-mail: mm@astro.soton.ac.uk

$$A(R) = +\frac{1}{2} \left(\frac{\Theta(R)}{R} - \frac{d\Theta(R)}{dR} \right) \quad (1)$$

$$B(R) = -\frac{1}{2} \left(\frac{\Theta(R)}{R} + \frac{d\Theta(R)}{dR} \right). \quad (2)$$

For a flat rotation curve we see that both A and B are inversely proportional to R , with smaller A and larger B values in the outer Galaxy. The quantity B is determined by studying the dependence of stellar proper motions on galactic longitude, while A can be calculated from analysis of either proper motions (μ_l) or radial velocities (v_r):

$$v_r = A d \sin 2l \quad (3)$$

$$\mu_l = \frac{A \cos 2l + B}{4.74}, \quad (4)$$

with d the distance to the object (in units of kpc), l Galactic longitude, A and B in $\text{km s}^{-1} \text{ kpc}^{-1}$, and μ_l in milli arcsec (mas) per year (Mihalas & Binney 1981). Note that the above equations for v_r and μ_l are only correct for $\frac{d}{R_0} \ll 1$.

It is also possible to determine $A - B = \Theta/R$ essentially independently from the individual values of A and B from proper motion surveys in the directions of $l = 90$ degrees and $l = 270$ degrees. In these directions, objects have a rather limited range in Galactocentric radius, and are thus only slightly affected by the radial dependence of the Oort functions.

Finally, the combination $-B/(A - B)$ can be estimated from the shape of the velocity ellipsoid of random stellar motions. Although the Oort *functions* vary with Galactic radius, stellar kinematic observations have only determined the Oort A and B *constants*, which are the values of these functions in the solar neighbourhood. Thus, in practice they tell us about the local shape of the rotation curve. However, it is important to note that the range over which the rotation curve parameters are effectively averaged depends on the range in Galactic radii over which the stellar observations are made.

The orbits of stars in the solar neighbourhood can be described as an epicyclic motion due to their random motions with respect the local standard of rest, superimposed on a circular orbit (Oort 1965). The length of the semi-major axis of the epicycle in the radial direction (a_{epi}) depends on the velocity in the radial direction (II):

$$a_{epi} = 0.5 \Pi / \sqrt{-B(A - B)}, \quad (5)$$

which equals ~ 350 , ~ 700 , and ~ 1200 parsec for Cepheids, early-type stars, and late-type stars, respectively. Thus, the random motions of stars introduces some form of radial smearing of kinematical properties which precludes significant variation of kinematical properties on scales smaller than a_{epi} .

Perhaps the greatest difficulty in interpreting the estimated values for the Oort constants comes from the presence of the derivative terms in equations (1) and (2): the values for the Oort constants depend on any local bumps and wiggles in the rotation curve as well as its global form. Any attempt to interpret the Oort constants must therefore consider the local topography of the rotation curve in the solar

neighbourhood. Unfortunately, the available observations of the Milky Way's rotational motion are not good enough to allow one to calculate the derivatives in $\Theta(R)$ directly from the data. Instead, some suitable functional form must be fitted to the data, and the derivatives of the model can then be calculated for comparison with the Oort constants.

The customary technique for fitting a model to rotation curve data for an external galaxy is to decompose the galaxy into different mass components: a stellar bulge and disk; an azimuthally-symmetric molecular and atomic gas disk; and a dark matter halo (e.g., van Albada & Sancisi 1986; Kent 1987; Begeman 1989; Lake & Feinswog 1989; Broeils 1992; Olling 1995; Olling 1996a). The free parameters in this mass decomposition are then constrained by requiring that the rotation curve for the model provides the best match possible to the observed kinematic data. In this paper, we seek to apply the same basic technique to the kinematic data for the Milky Way in order to produce a dynamical picture consistent with the observed Oort constants.

Although the dominant contributors to the total mass come from the stellar components and the dark halo, the contribution from the gas cannot be neglected in this application. While the stars and dark matter are believed to be fairly smoothly distributed with radius, the distribution of molecular and atomic hydrogen (H_2 and H I respectively) often show density enhancements like rings and arms. Such irregular distributions will produce a contribution to the total rotation speed that can vary non-monotonically with radius. Thus, although these components do not contribute much to the amplitude of the rotation curve, they can have a large effect on its local derivative, and hence the predicted values of the Oort constants.

We start by presenting the Milky Way's 'observed' rotation curve and its uncertainties in §2. In section 3, we calculate the radial distribution of gas in the Milky Way, and show that it does, indeed, significantly affect the analysis of the Oort constants. Section 4 presents the mass component decomposition of the Milky Way's rotation curve, and shows that the resulting models are completely consistent with the constraints from the Oort constants as long as we adopt values for R_0 and Θ_0 at the lower end of the acceptable range. In section 5, we discuss the implications of these results. And we summarize in section 6.

2 THE MILKY WAY'S ROTATION CURVE

We have constructed the rotation curve of the inner Galaxy from the tangent point measurements (Malhotra 1995). For the outer Galaxy, we have used determinations of the $W(R)$ curve [Eqn. (6)] based on H_2 regions (Brand & Blitz 1993) and the thickness of the gas layer (Merrifield 1992). As mentioned in the introduction, the rotation curve inferred from radial velocity observations depends significantly on the adopted values of Θ_0 and R_0 , and so we constructed about 50 "observed" rotation curves for 5 choices of R_0 (6.1, 6.8, 7.1, 7.8, and 8.5 kpc) and about 10 values of Θ_0 between 170 and 230 km s^{-1} . All of these rotation curves are consistent with the observed radial velocity measurements in the inner and outer Galaxy. Generally speaking, small values for Θ_0 and/or R_0 yield declining or flat rotation curves, while the rotation curves constructed for large Θ_0 and/or

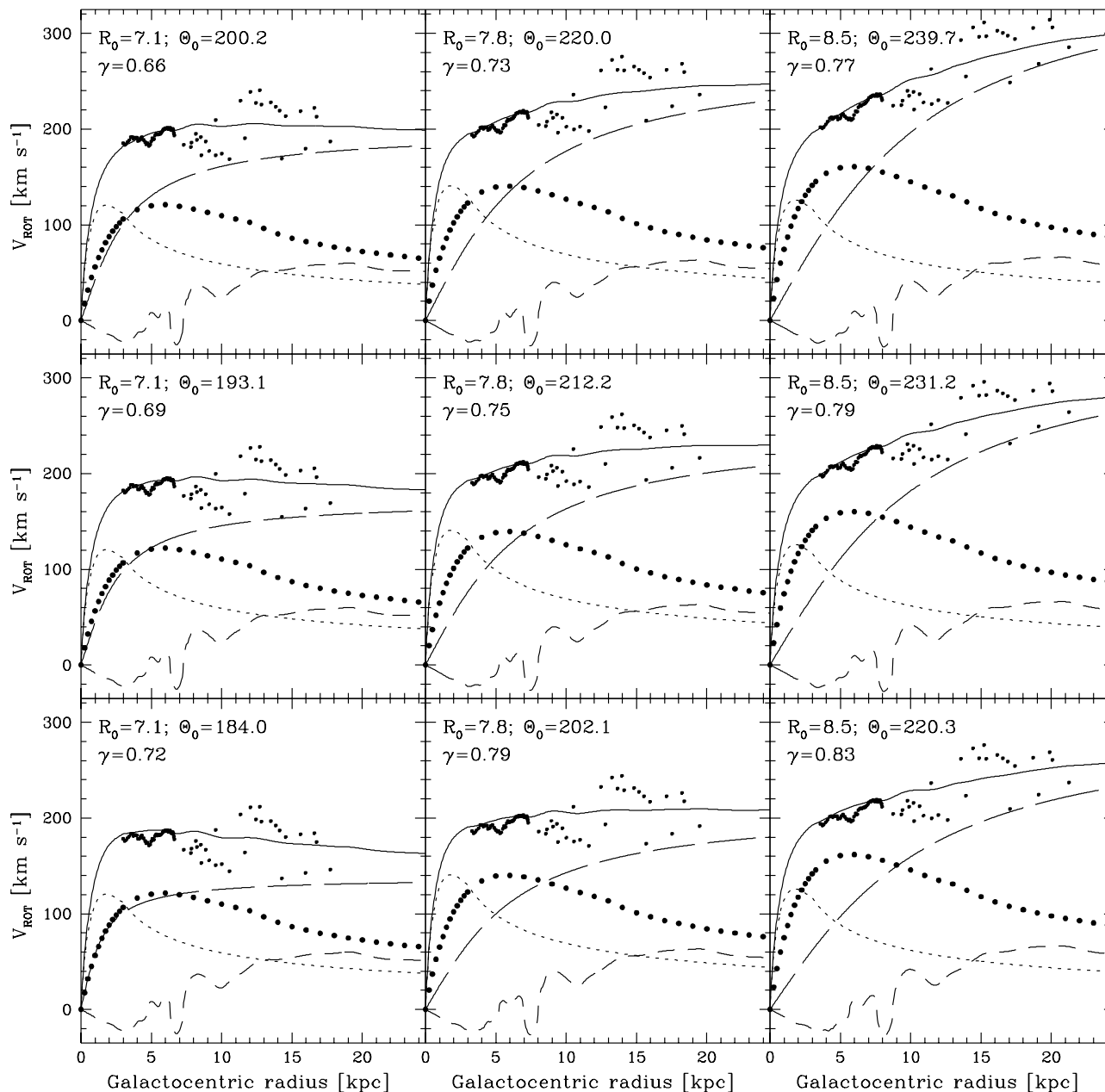


Figure 1. Nine possible rotation curves (dots) for the Milky Way which are consistent with the tangent point data (Malhotra 1995), the radial velocities of H II regions (Brand & Blitz 1993) and the H I $W(R)$ curve (Merrifield 1992). For clarity, we did not plot the error bars on the observed data points (a few km s^{-1} , and $\sim 15 \text{ km s}^{-1}$ in the inner and outer Galaxy, respectively). Each panel corresponds to a different choice for R_0 and Θ_0 , where all R_0 - Θ_0 combinations are consistent with the Kerr & Lynden-Bell values at the $1.3\text{-}\sigma$ level. From left to right the Galactocentric distance R_0 increases from 7.1 through 7.8 to 8.5 kpc. In the bottom row we present our best-fitting model (left panel; $R_0 = 7.1$ kpc, $\Theta_0 = 184 \text{ km s}^{-1}$, $A-B = 25.92 \text{ km s}^{-1} \text{ kpc}^{-1}$; see §5), Sackett's suggested values (middle panel; 1997), and Kerr & Lynden-Bell's recommendations (right panel; 1986). From bottom to top ($A-B$) increases from our best fitting value of $(A-B) = 25.92 \text{ km s}^{-1} \text{ kpc}^{-1}$, through Feast & Whitelock's (1997) best fit value $(A-B)_{FW} = 27.2 \text{ km s}^{-1} \text{ kpc}^{-1}$, to $(A-B) = (A-B)_{FW} + 1\text{-}\sigma = 28.2 \text{ km s}^{-1} \text{ kpc}^{-1}$. For smaller values of $(A-B)$ and/or R_0 , the rotation curve will decline even more with radius. The mass model fit to the rotation curve is shown as a solid line (§4.1). Also shown are the contributions from the individual components: the bulge (dotted line); the stellar disk (filled circles); the dark halo (long dashed line); and the gas layer (short dashed line). Notice that the contribution of the dark halo increases for smaller values of R_0 and larger rotation speeds. The degree to which the disk is maximal (γ ; Olling 1995) is indicated in each panel. Note that the total *stellar matter* (Sackett 1997) contributes somewhat more: $\sim 74\%$, $\sim 81\%$, and $\sim 81\%$ for $R_0 = 7.1$, 7.8, and 8.5 kpc, respectively. The non-linear behaviour of the rotation curve due to the gas in the Solar neighbourhood introduces a tiny wiggle in the total model rotation curves, similar effects are seen around $R = 0.6R_0$ and $1.4R_0$.

R_0 values tend rise in the outer Galaxy. Figure 1 shows some typical models.

A comparison of the Galactic rotation curve with rotation curves of external galaxies is best made when the radial extent is re-scaled in terms of the optical scale-length ($h_R = 2.5 \pm 0.5$ kpc; §4.1). The last measured point on the Milky Way's rotation curve lies at $2R_0$, so that the extent falls somewhere between approximately $4.7h_R (= 2 \times 7.1/3)$ and $8.5h_R (= 2 \times 8.5/2)$. It is not uncommon for galaxies to have rotation curves which decline somewhat between a peak at around $2.3h_R$ and $5h_R$. This is in particular common in systems with large bulge-to-disk ratios[‡] like M31 (Kent 1989), NGC 2683 & NGC 3521 (Casertano & van Gorkom 1991), and many others (Rubin et al. 1985; Beegman 1987; Broeils 1992). In terms of the universal rotation curve (Persic, Salucci & Stel 1996), 200 km s^{-1} is a dividing point: on average, systems which rotate faster decline beyond $2.3h_R$, while for slower rotators the trend is to have a rising rotation curve. From the comparison with external galaxies we conclude that $\Theta_0 = 180 \pm 20 \text{ km s}^{-1}$, while a rotation speed at the solar circle as high as 220 km s^{-1} is highly unlikely (see also Merrifield 1992).

The accuracy of the Milky Way's rotation curve – reflected by the scatter of the data points in Fig. 1 – is much poorer than that routinely obtained for external galaxies. This is partly explained by the fact that for external galaxies a large range in azimuth can be used, while for the Milky Way only two regions in Galactocentric longitude around $l = 135^\circ$ and $l = 225^\circ$ [cf. Eqn. (3)] are useful. Only in those regions is the v_r -distance gradient large enough to rise above the noise induced by the tracer's random motions. Furthermore, small errors in the tracers distances or small non-circular motions in regions away from $l = 135^\circ$ and $l = 225^\circ$ can result in large changes in the inferred rotational velocities. Clear examples of this effect are the deviant points on our rotation curve between 1 and $1.2R_0$ which arise from radial velocities of H_2 regions between $l = 90^\circ$ and $l = 120^\circ$ (Brand & Blitz 1993). These data points are likely to be affected by non-circular motions (Dehnen & Binney 1997) induced by the nearby Perseus arm (Brand & Blitz 1993), and distance errors resulting from unaccounted for extinction, or errors in the photometric parallaxes (Oudmaijer, private communications). These large errors preclude the determination of the Oort constants from the Milky Way's observed rotation curve. As the best alternative, we will model the rotation curve and determine the Oort constants from the smooth model fits instead. Rather than using the customary linear or power-law fits to the rotation curve, we use the mass modeling procedure which has proven highly successful in external galaxies (§4.1).

3 THE H I AND H_2 DISTRIBUTIONS

In order to determine the radial variation of the column density of the molecular and atomic hydrogen, we need to be able to assign a distance to a parcel of gas observed at

[‡] The Milky Way's bulge-to-disk ratio is approximately 0.27, in K-band (Olling & Merrifield 1998a)

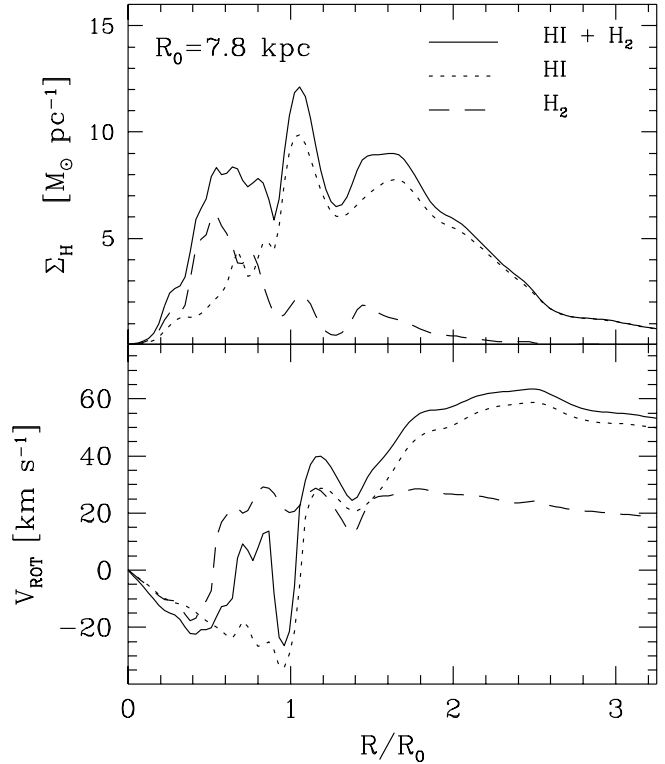


Figure 2. The upper panel shows the face-on surface density distribution of the H I (dotted line), the H_2 (dashed line), and the sum of two (full line) for the Milky Way. The lower panel shows the contribution these components make to the circular speed of the Galaxy, where a negative rotational velocity means that the radial force is directed outwards. For other values of R_0 , the surface density is unaffected, but the rotation speeds vary approximately proportional to R_0 . The radial force due to the ISM varies strongest in the regions around $0.6R_0$, R_0 , and $1.4R_0$.

Galactic coordinates l and b , and radial velocity v_r . Assuming that the gas is on a circular orbit, its distance d can be determined using the following relations:

$$W\left(\frac{R}{R_0}\right) = \frac{v_r}{\sin l \cos b} = \frac{R_0}{R} \times \Theta\left(\frac{R}{R_0}\right) - \Theta_0, \quad (6)$$

$$R^2 = R_0^2 + d^2 \cos^2 b - 2R_0 d \cos l \cos b. \quad (7)$$

While the radial velocity and $W(\frac{R}{R_0})$ can be determined accurately (Malhotra 1995; Merrifield 1992; Brand & Blitz 1993), the uncertainties in R_0 and Θ_0 lead to a significant uncertainty in the value of d . We have therefore performed this analysis using a range of values for R_0 and Θ_0 . Using the rotation curves which follow from the adopted values for R_0 and Θ_0 , we determined the volume and column densities of the molecular and atomic gas. For the inner Galaxy, the H I column density was determined from the midplane volume density (Burton 1988) and the observed thickness of the layer (Malhotra 1995). The column densities for $R \geq R_0$ were taken from Wouterloot et al. (1990), with $9.25 M_\odot \text{ pc}^{-2}$ at the Solar circle. The H_2 column densities for the inner and

outer Galaxy were taken from Bronfman et al. (1988) and Wouterloot et al. (1990), respectively. The column density of H_2 at the solar circle is $1.8 M_\odot \text{pc}^{-2}$, and so, neglecting the column density due to the other phases of the ISM, we arrive at a total column density for the ISM at the solar circle of $14.5 M_\odot \text{pc}^{-2}$, which includes 23.8% Helium by mass (Olive & Steigman 1995). Note that while the column density at fractional radius R/R_0 is independent of the choice of R_0 (Bronfman et al. 1988), the Milky Way's total gas mass does depend on this value.

The H I and H_2 column densities, and these mass components' contributions to the total rotation curve, are presented in Fig. 2. It is apparent that the sun resides in a part of the Milky Way where the gradient of the gas column density is substantial, and that their corresponding contributions to the gradient in the rotation curve are large. Clearly, this effect must be taken into account when interpreting the Oort functions of equations (1) and (2).

Note however that this effect is not limited to the Solar neighbourhood: the regions around $0.6R_0$ and $1.4R_0$ exhibit similar behavior. Examples of such non-monotonic rotation curves and H I surface density distributions can be found in many external galaxies (Begeman 1987). Some galaxies which have been observed with high linear resolution show strong radial H I density gradients: NGC 4244 (Olling 1996a), NGC 891 (Becquaert, Combes & Viallefond 1997), M31 (Brinks & Burton 1984), M33 (Deul & van der Hulst 1987), and NGC 1560 (Broeils 1999b) all show similar radial density gradients to those found in the Milky Way.

4 ROTATION CURVE, MASS MODELS AND THE OORT CONSTRAINTS

In order to produce a complete mass model for the Milky Way, we must fit all the components – gas, stars and dark matter – to the observed rotation curve.

4.1 Mass models

In a previous section, we obtained the gas mass distribution, so we now turn to the stars and dark matter. We have modeled the stellar component as the sum of a bulge and disk, whose light distribution is consistent with Kent's (1992) photometry, with the disk scalelength forced to lie in the range $h_R=2.5 \pm 0.5$ kpc (Sackett 1997). The dark halo was modeled as a non-singular isothermal sphere. We refer the reader to a related paper (Olling & Merrifield 1998a) for a more detailed description of the mass models.

We then solved for the free parameters in this model by fitting the observed rotation curve to the predictions of the mass model. This procedure that has been followed in many previous analyses (Caldwell & Ostriker 1981; Bahcall, Schmidt & Soneira 1983; Rohlfs & Kreitschmann; Kuijken & Gilmore 1989; Kent 1992; Merrifield 1992; Evans & Jijina 1994; Alcock et al. 1995; Gates, Gyuk & Turner 1995; Dehnen & Binney 1997), but, to our knowledge, none of the previous studies have included the actual radial surface density distribution of the Milky Way's ISM. In addition, we imposed the constraint that the mass model had to reproduce the observed stellar surface density of the Milky Way

in the solar neighbourhood, $\Sigma_* = 35 \pm 5 M_\odot \text{pc}^{-2}$ (Kuijken & Gilmore 1989).

For each of the 50 R_0 - Θ_0 combinations considered, we constructed nine mass models with $h_R=2, 2.5,$ and 3 kpc, and three stellar mass-to-light ratios (Υ_*) such that Σ_* is recovered to within $\pm 1\text{-}\sigma$ (Olling & Merrifield 1998a). We show nine of the ~ 450 mass models – chosen to be representative of the ensemble – in Figure 1.

4.2 Oort constants constraints

From each mass model, we can calculate directly the Oort functions, $A(R)$ and $B(R)$, as defined by equations (1) and (2). Figure 3 shows these functions for models obtained from three combinations of R_0 and Θ_0 . It is clear that the Oort functions (and the various combinations thereof) vary significantly over even the limited range of radii shown. In the Solar neighbourhood about half of the variation in $A(R)$ and $B(R)$ can be attributed to the general $\Theta(R)/R$ trend (dotted lines), while the local deviations are caused by the contribution of the gaseous component to the rotation curve. It is also apparent that the values of these functions vary significantly over the acceptable range of values for R_0 and Θ_0 .

The functions also change to some extent when we adopt different acceptable combinations of the other parameters in the mass model (h_R , Υ_* , and the parameters of the dark halo). However, these modifications are all small. The error bar toward the right of each panel in Figure 3 indicates the full range of variations induced by such changes. Since the acceptable combinations of stellar and dark matter components all reproduce the same large-scale smooth variation with radius of the rotation curve, the resulting Oort functions scarcely depend on the particular combination adopted. The dependence on R_0 and Θ_0 arises because changing these quantities alters the largescale shape of $\Theta(R)$ (see Fig. 1). Thus, although the observed values for various Oort constraints will not distinguish between the details of the various degenerate mass models, they will allow us to decide which combinations of R_0 and Θ_0 are consistent with the observed stellar kinematics.

The observed values for the various Oort constraints, taken from Kerr & Lynden-Bell (1986; hereafter referred to as KLB86) and Hanson (1987; henceforth H87) are summarized in Table 1, and are also plotted in Figure 3. Since the Oort functions vary substantially with radius, it is vital that we compare the observed values to the functions over the appropriate range of radii. If we had not included the contribution from the gas component (dotted lines in Figure 3), the Oort functions $A(R)$ and $B(R)$ would have changed steadily with Galactocentric radius [$dA/dR \sim -1.9, dB/dR \sim 2.5$ ($\text{km s}^{-1}\text{kpc}^{-1})/\text{kpc}$]. However, the contribution of the gas flattens the A and B gradients substantially over the scale of the width of the H I crest which peaks at $1.1R_0$. In this radial regime we can thus use the small distance approximations – which require constant A and B values – for v_r and μ_i [Eqns. (3) and (4)].

Unfortunately, KLB86 obtained their estimates by averaging together a number of previous determinations, and it is not clear what range in radii the data for these various analyses came from. As KLB86 noted, it is even unclear if the individual estimates were all obtained from data at

Table 1. The Oort Constants as determined by several groups: KLB86 (Kerr & Lynden-Bell 1986), PMB94 (Pont, Mayor & Burki 1994), BB93 (Brand & Blitz 1993), and FW97 (Feast & Whitelock 1997). We adopt the values as determined by H87 (Hanson 1987). The units of A , B , $(A - B)$, and $(A + B)$ are $\text{km s}^{-1} \text{kpc}^{-1}$, R_0 is in kpc, and Θ_0 in km s^{-1} . The ratio $-B/(A - B)$ may be equated with the square of the tangential to radial stellar velocity dispersion ($X^2 = \sigma_\phi^2/\sigma_R^2$). Most stars of spectral type G through K fall in the “low X^2 ”. M type stars fall mostly in the “high X^2 ” category (see §4.2).

	A	$-B$	$A - B = \Theta_0/R_0$	$A + B = (d\Theta/dR) _{R_0}$	$\frac{-10B}{A-B}$	R_0	Θ_0
KLB86	14.5 ± 1.3	12.0 ± 2.8	26.4 ± 1.6	$+2.5 \pm 3.1$	4.2 ± 0.6	8.5 ± 1.1	220 ± 20
BB93	12.6	13.2	25.9	-0.6	5.1	8.5	220
PMB94	15.9 ± 0.3					8.1 ± 0.3	
FW97	14.8 ± 0.8	12.4 ± 0.6	27.2 ± 1.0	$+2.4 \pm 1.0$	4.5 ± 0.2	8.5 ± 0.5	231 ± 15
H87	11.3 ± 1.1	13.9 ± 0.9	25.2 ± 1.9	-2.6 ± 1.4	5.5 ± 0.5		
This work	11.3 ± 1.1	13.9 ± 0.9	25.2 ± 1.9	-2.6 ± 1.4		7.1 ± 0.4	184 ± 8
low X^2					3.5 ± 0.5		
high X^2					5.0 ± 0.5		

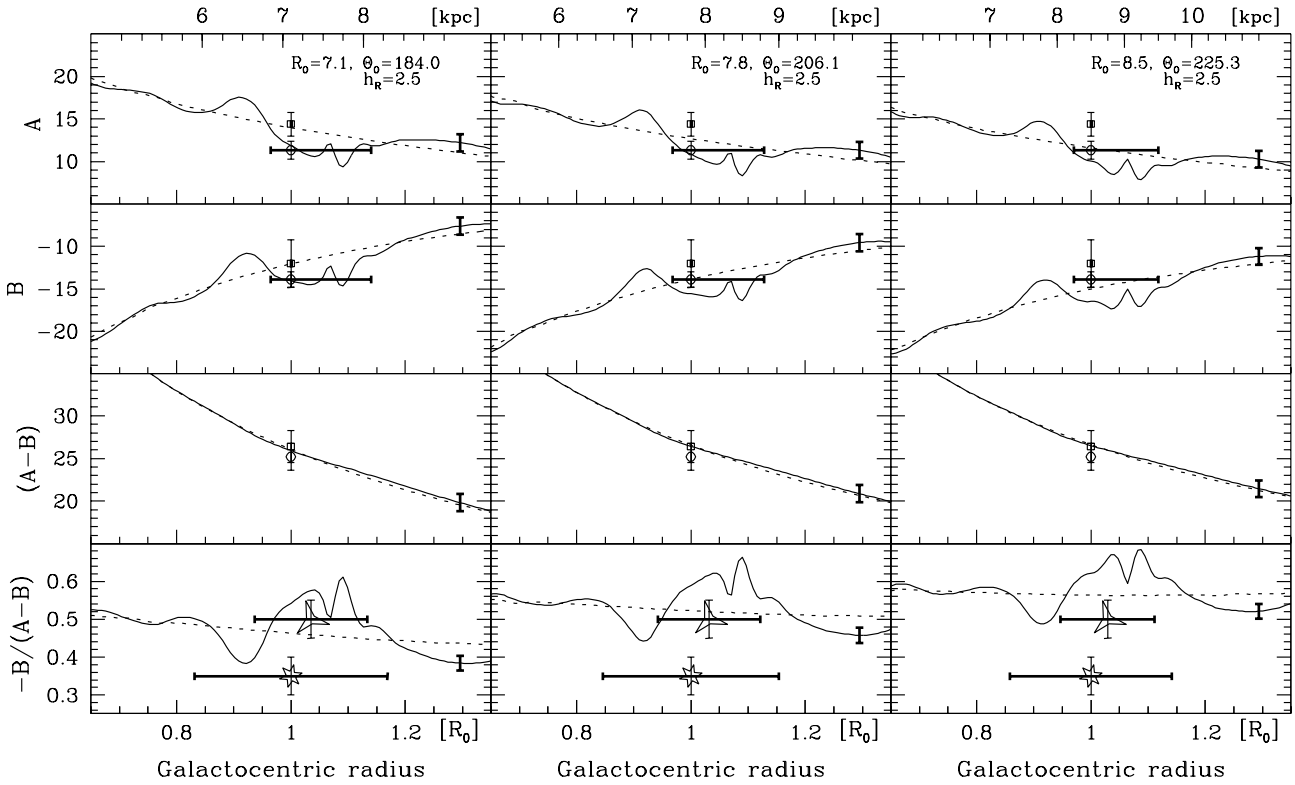


Figure 3. The Oort functions, $A(R)$ and $B(R)$, as derived for three model rotation curves, together with the values of $(A - B)$ and $-B/(A - B)$. The units for A , B , and $(A - B)$ are $\text{km s}^{-1} \text{kpc}^{-1}$. The solid lines show the Oort functions as derived from the full mass model, while the dashed line shows what happens if the gas component is ignored. The error bar at the right of each panel shows the range of uncertainty due to variations in the other model parameters (T_* and h_R). The various observational estimates of these quantities are also shown, with the horizontal error bars indicating the radial range over which the observations effectively averaged (see text for details). The upper three panels show values as determined by KLB86 (open squares) and H87 (open circles). The bottom panels show the values of $-B/(A - B)$ as predicted by the velocity dispersions of “high X^2 ” stars (M dwarfs and G-M giants; triangles) and “low X^2 ” stars (G-K dwarfs; hexagons).

commensurate radii. We are therefore unable to estimate the appropriate radial range for these estimates. H87 used a more consistent set of data from the Lick Northern Proper Motion survey, consisting of 60,000 stars within about 1 kpc of the Sun. From their $B - V$ colors [0.84 ± 0.5 , (Klemola,

Jones & Hanson 1987)] we infer that these stars are F2-K0 dwarf stars (Mihalas & Binney 1981) with a radial dispersion of roughly 29 km s^{-1} , so that the epicyclic radius for these stars is $\sim 780 \text{ pc}$ [cf. Eqn. (5)]. The Galactic longitudes of these stars ($l \approx 50 - 195$ degrees; $|b| \geq 10^\circ$) indicate that

they are mostly located in the outer Galaxy: the horizontal bar on the H87 data points in Figure 3 represents the range of R of a typical star in this sample [$(R_0 - 250, R_0 + 1000)$ parsec]. Since this region roughly equals the area which is covered by the epicyclic motions of these F2-K0 dwarfs, they can be used to determine intrinsic Galactic properties on this scale. Furthermore, as discussed above, Hanson’s use of the approximate μ_l relation [Eqn. (4)] is justified due to the flatness of the $A(R)$ and $B(R)$ functions in this region.

From Figure 3 it is clear that the values of A and B derived by H87 are consistent with the Oort functions for small values of R_0 and Θ_0 . Models without the contribution from the gas component yield larger values for A and B . It is also noteworthy that the value of $2AR_0$ based on determinations of $W(R)$ in the inner Galaxy is 1.4 ± 0.25 times larger than the value determined in the outer Galaxy (Merrifield 1992); this finding is also entirely consistent with the Oort A -function curves shown in Figure 3.

An independent estimate for $(A - B)$ comes from proper motion surveys in the directions $l = 90$ degrees and $l = 270$ degrees. Objects in these directions lie at radii close to R_0 out to quite large distances, and so no radial range is plotted for the KLB86 and H87 estimates for this quantity in Figure 3. In any case, the absence of a $d\Theta/dR$ term in this combination of Oort functions means that $(A - B)$ is a smooth function of radius, so the importance of knowing the precise radial range of the determination is reduced. Once again, the H87 value for $(A - B)$ is best matched by models with small values of R_0 and Θ_0 .

Finally, we turn to the observed value of $-B/(A - B)$. If the potential is azimuthally symmetric and the velocity dispersions are small, then this combination of the Oort parameters is equal to the square of the ratio of the tangential and radial stellar velocity dispersions, $(\sigma_\phi/\sigma_R)^2$ (Kuijken & Tremaine 1994). The accepted value for this ratio is $X^2 = (\sigma_\phi/\sigma_R)^2 = 0.42 \pm 0.06$ (Kerr & Lynden-Bell 1986). However, upon close examination there appears to be a bimodal distribution in X^2 : dwarfs of spectral type G-K have a low value [$X_{D,G-K}^2 = 0.36 \pm 0.07$], while M dwarfs and G-M giant stars have a somewhat larger dispersion ratio ($X_{D,M}^2 = 0.5 \pm 0.11$, and $X_{G,M}^2 = 0.5 \pm 0.07$; (Delhaye 1965, henceforth D65, and references therein; Mihalas & Binney 1981)]. In fact, the large error on $X_{D,M}^2$ arises as a result of the bimodality in the distribution of X^2 (Reid, Hawley & Gizis 1995; $X_{low}^2 = 0.36$, $X_{high}^2 = 0.48$), which is also clearly seen in the distribution of space motions of individual stars (Vyssotsky & Janssen 1951; Delhaye 1965, and references therein; Delhaye 1965, Fig. 2; Mihalas & Binney 1981, Figs. 7.1 & 7.3). Furthermore, these figures show that the giant stars have a bimodal distribution as well. This result was confirmed by more recent investigations (Mayor 1974; Oblak 1983), which found a minimum dispersion ratio for stars ~ 1 Gyrs old ($X^2 \sim 0.36$) while the dispersion ratios for older and younger stars are larger ($X^2 \sim 0.46$). Thus, rather than having to account for the average X^2 -value of 0.42 ± 0.06 , we are faced with the task to explain the bimodal X^2 distribution. We estimate the location of the two peaks to lie at: $X^2 = 0.35 \pm 0.05$, and $X^2 = 0.5 \pm 0.05$. Figure 3 suggests that these results can be explained if the bimodality in the dispersion-ratio measurements is a result of the “dip” and the “hump” in the $-B/(A - B)$ curve around $0.9R_0$ and $1.1R_0$, respectively.

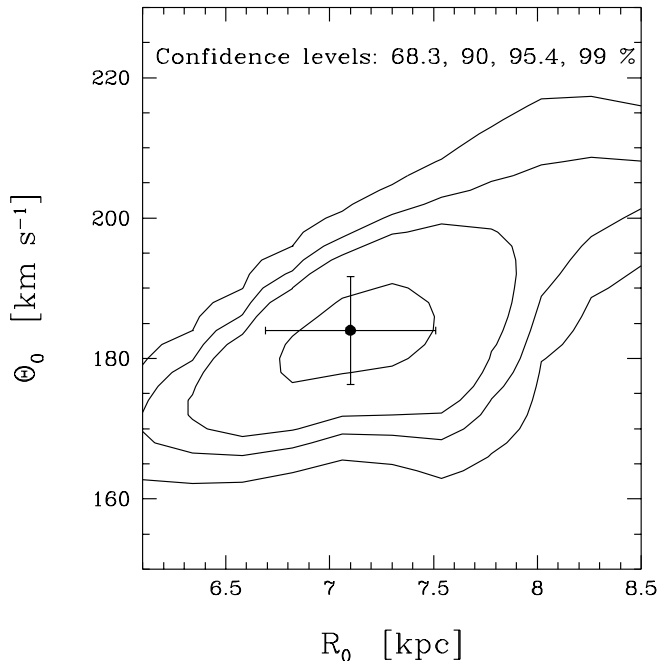


Figure 4. The contours of equal likelihood as a function of R_0 and Θ_0 , calculated by comparing stellar kinematic constraints to the model-predicted Oort constants. The best-fit minimum- χ^2 values for R_0 , Θ_0 , and their 1- σ errors are also indicated.

In this scenario, the dwarf sample is dominated by stars originating within the Solar circle (small X^2 values) with a smaller number of dwarf showing the larger X^2 -value, while the giants used in the dispersion measurements come preferentially from the outer Galaxy. Since the stellar density increases towards smaller R with a scale-length that may be as small as 2 kpc, and since the observed distribution of giants is concentrated around $(R - R_0) = 250$ pc (McCuskey 1965), this may well be the case. The larger range in radii covered by the dwarf stars with their larger epicyclic excursions (indicated by the horizontal bars on the points in Fig. 3) also means that these stars are more influenced by the dip in the $-B/(A - B)$ curve at $R \approx 0.9R_0$, explaining the lower observed average value. Once again, only models with low values of R_0 and Θ_0 are consistent with the observations.

5 DISCUSSION

It is apparent from the above analysis that the local topography of the rotation curve induced by the small-scale structure in the gas component has a significant impact on the interpretation of the stellar-kinematic Oort constraints. Once this phenomenon is taken into account, it is possible to obtain model rotation curves for the Milky Way that are consistent with essentially all the Oort constraints.

It is also clear from Figure 3 that a consistent picture only emerges for certain values of R_0 and Θ_0 . We can formalize the constraints that this analysis puts on the values of the

Galactic constants by calculating a χ^2 statistic comparing the observed combinations of the Oort constants in Figure 3 to the values predicted by the models. Since this comparison requires that we know the radial range over which the observations have been made, we use the observations plotted in Figure 3 for which we have an estimate of this range (see above), together with the H87 estimate for $(A - B)$.

The χ^2 statistic comparing these five observations to suitably radially-averaged models were then calculated for a range of values for R_0 and Θ_0 . The best-fit (minimum- χ^2) values for these parameters are $R_0 = 7.1 \pm 0.4$ kpc, and $\Theta_0 = 184 \pm 8$ km s $^{-1}$. The complete two-dimensional confidence regions are plotted in Figure 4. The confidence levels measure the probability that any given values for R_0 and Θ_0 are consistent with the observed Oort constraints. Thus, for example, the official IAU-sanctioned values of $R_0 = 8.5$ kpc and $\Theta_0 = 220$ km s $^{-1}$ are ruled out at the 99% confidence level. It is, however, notable that a value for R_0 as low as 7.1 kpc is entirely consistent with the only *direct* distance determination to the Galactic center employing proper motions of H $_2$ O masers, $R_0 = 7.2 \pm 0.7$ kpc (Reid 1993).

The proper motion of Sgr A*, μ_{SgrA^*} (Backer & Sramek 1987; Backer 1996; Reid 1998), has been used to constrain $(A - B)$ as well (Gould & Ramirez 1997). These quantities are related via the formula,

$$\mu_{SgrA^*} = -\frac{A - B}{4.74} - \frac{v_0 + v_{SgrA^*}}{4.74R_0} \text{ milliarcsec year}^{-1}, \quad (8)$$

where v_0 is the Solar motion relative to the local standard of rest ($v_0 = 5.3 \pm 1.7$ km s $^{-1}$; Binney et al. 1997) and v_{SgrA^*} is the velocity of Sgr A* with respect to the Galactic centre ($v_{SgrA^*} \leq 11$ km s $^{-1}$; Gould & Ramirez 1997). Using the range of acceptable values for $(A - B)$ derived from our mass models, we find that the proper motion of Sgr A* should lie in the range $\mu_{SgrA^*} = -5.95 \pm 0.36$ milliarcsec per year, which is entirely consistent with the observational constraints.

5.1 Other determinations of the Galactic constants

Inspection of Table 1 reveals that the Oort constants as derived by different authors can vary by up to 4.2- σ . We have used the determination of the Oort constants which are based on ground based proper motions of relatively nearby stars ($d \leq 1$ kpc; H87) in the outer Galaxy. Cepheids probe a much larger range in distance and can be used to determine the Oort constants as well, but yield significantly different values (Pont, Mayor & Burki 1994, henceforth PMB94; Feast & Whitelock 1997, hereafter referred to as FW97).

Let us first examine the region within 1 kiloparsec from the Sun where the non-linearity of the Oort functions is most prominent. As discussed above, the H87 determined A and B in the ‘‘flat’’ region extending from $0.95R_0$ to $1.15R_0$: $A_{H87} = 11.3 \pm 1.1$ km s $^{-1}$ kpc $^{-1}$. The Cepheids on the other hand are located preferentially in the inner Galaxy (PMB94, their Fig. 4) where our models yield an average A of 15.4 ± 2 , entirely consistent with their value of 15.9 ± 0.3 . From Figure 3 it is also clear that beyond 1 kpc the non-linearities in $A(R)$ and $B(R)$ are much smaller. In order to assess whether the PMB94 & FW97 results are consistent with our models at large distances, we have compared the radial velocities

and proper motions as predicted by the PMB94 & FW97 models with our models. Since the PMB94 & FW97 models are fitted directly to their data, we are in effect comparing our models with their data. Our model rotation curves yield exact radial velocities with equation (6), and exact proper motions using the formula

$$\mu_l = \left(\frac{\Theta(R)(R_0 \cos l - d) \cos b}{R} - \Theta_0 \cos l \right) \frac{1}{4.74d}, \quad (9)$$

in units of milli arcsec per year, with the distances in units of kiloparsec (Mihalas & Binney 1981). In the upper panels of Fig. 5 we present the proper motion curves as modeled by FW97 (symbols) and some of our models (lines) for a range of values for R_0 , Θ_0 , and d . In the bottom panels we plot the difference between the two. Our model which best fits the Oort constant constraints ($R_0=7.1$ kpc, $\Theta_0=184$ km s $^{-1}$) is displayed in the leftmost column; the agreement between the FW97 proper motions and our predictions is excellent. The worst agreement between data and model is found for large distances towards the Galactic centre, where the rotation curve is rather ill-defined as a result of bar-induced non-circular motions. Furthermore, we note that models with larger and smaller values for R_0 fit the FW97 data progressively worse. We draw the same conclusion from a similar comparison of the PMB94 radial velocity data with our models.

From Figure 5, we can also see that the vertical scatter seen in observational $l - \mu_l$ plots is not due to some intrinsic scatter, but rather results from the fact that the data occupy a finite range in radii. Clearly the approach followed by PMB94 & FW97 – fitting model v_r and μ_l curves which include distance effects – is superior to the application of the approximate equations [Eqns. (3) and (4)].

Given that the best-fit values of the Galactic & Oort constants in this analysis are so different from the Cepheid derived values it behooves us to explain why our best model nevertheless is able to fit the radial velocity and proper motion data (Fig. 5) so well. The reason for this is that the Milky Way’s rotation curve and the Galactic & Oort constants are secondary parameters: a wide range in secondary parameters is consistent with the primary observable $W(\frac{R}{R_0})$ (Fig. 1). So assuming that the $W(\frac{R}{R_0})$ curves as measured by Brand & Blitz (1993), Merrifield (1992), and Pont, Mayor & Burki (1994) are a fair sample of the intrinsic Galactic velocity field, it is not surprising that our smooth model fits to the first two data sets are consistent with PMB94’s Cepheids data. Varying the Galactic constants has only a small effect on the proper motions, as can be seen by rewriting equation (9) in terms of the primary observable $W(\frac{R}{R_0})$:

$$\mu_l = \frac{1}{4.74} \left(\frac{W(\frac{R}{R_0}) \cos l}{d} - \frac{W(\frac{R}{R_0})}{R_0} - (A - B) \right). \quad (10)$$

Changing $(A - B)$ shifts the μ_l curves up and down, but the observed error on $(A - B)$ corresponds to a small vertical shift of μ_l , which is only significant in the Galactic centre and anti-centre regions. Likewise, changing R_0 affects the ratio $\frac{R}{R_0}$ – and hence W – only slightly [through Eqn. (7)]. Like a change in $(A - B)$, adjusting R_0 shifts the μ_l curves up and down. The only longitudinal dependence comes from the

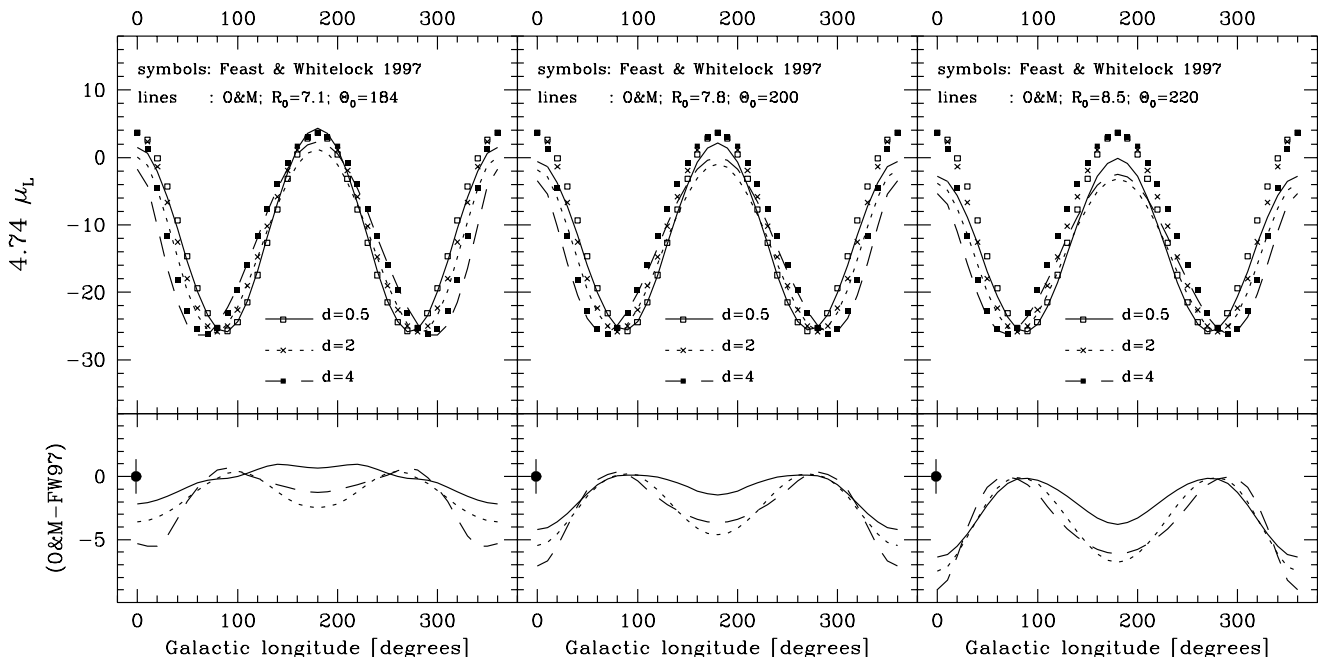


Figure 5. Proper motions (top row) as calculated using the Oort and Galactic constants derived by FW97 ($R_0 = 8.5$ kpc, $A = 14.82$, $B = -12.37$ km s $^{-1}$, and $d^2\Theta/dR^2 = d^3\Theta/dR^3 = 0$), and some of our models. In the lower panels we display the difference between the proper motions predicted by our models and those predicted by FW97. The units for the vertical axes are km s $^{-1}$ kpc $^{-1}$. All curves were calculated for $b = 0$. The error bar in the bottom panel equals the quadratic sum of the errors of FW97’s determinations of A and B . In the leftmost panel we present our model which best fits the Oort constants constraints ($R_0 = 7.1$ kpc, $\Theta_0 = 184$ km s $^{-1}$), while the other two panels were calculated for the Sackett (1997; middle panels) and Kerr & Lynden-Bell (1986; right columns) recommendations for the Galactic constants. Again, worse correspondence between models and “data” occurs if $(|R_0 - 7.1|)$ increases. In our models, assuming a different value for Θ_0 will shift the μ_l curves slightly up or down by $\Delta\Theta_0/R$.

first term, which can be large for small distances d . Thus, the differences between the proper motion curves for different choices of R_0 & Θ_0 in Fig. 5 are not very large. However, the residuals *do* increase if either R_0 or Θ_0 or both are adjusted: our preferred model fits the proper motion data best.

5.2 Uncertainties in the $W(R)$ curve

The derived form for the Galactic rotation curve depends on the adopted $W(R)$ curve. In this paper, we have based our analysis on the radial velocities of H II regions (Brand & Blitz 1993) and the H I $W(R)$ curve (Merrifield 1992). However, one could also infer this curve from radial velocities of Cepheids. As Dehnen & Binney (1997) have noted, the $W(R)$ curve derived from Cepheids drops significantly more rapidly with R than that obtained from the data sets exploited here. For such a rapidly-falling form for $W(R)$ to produce a reasonably flat rotation curve, one must adopt a large value of Θ_0 . It is, therefore, unsurprising that Metzger, Caldwell & Schechter’s (1998) analysis of Cepheid kinematics results in models of the Milky Way with Θ_0 as high as 240 ± 10 km s $^{-1}$. Their modeling obtained a value for R_0 of 7.7 ± 0.3 kpc; the corresponding value for $(A - B) = \Theta_0/R_0$ is 31 ± 2 km s $^{-1}$ kpc $^{-1}$, which is inconsistent with the various stellar kinematic constraints summarized in Table 1.

Clearly, these internal inconsistencies mean that there

must be systematic errors in at least some of the available data. The unknown nature of these errors means that there can be no objective criterion for choosing between the various methods. The only way that a final answer can be reached will be from the analyses of other kinematic tracers. Through such studies, one might hope to identify and prune the discrepant data sets, obtaining a consistent picture from the remaining majority. With only three “reliable” techniques for obtaining $W(R)$, we are not yet in a position to carry out such a democratic procedure.

5.3 The effects of non-circular motions

One potential source of error in this analysis comes from our assumption that the orbital structure of the Milky Way has an azimuthal symmetry. The presence of spiral structure means that this assumption is almost certainly an oversimplification. Non-circular motions will have two effects on the above analysis.

First, in Section 3 we used kinematic distances to derive the distribution of gas. These distance assume that the gas follows circular orbits, and so the inferred distribution will be distorted if there is significant non-circular streaming. However, dynamical models of spiral structure show that the locations of high density ridges are quite accurately reproduced by the naive kinematic modelling, and so the ra-

dial positions of the density peaks and troughs apparent in Figure 2 should be approximately correct, and the conclusion that we are located in a region where this density varies rapidly with radius still holds. Second, the non-circular motions hamper the determination of the intrinsic $W(R)$ curve from which the rotation curve, the Oort constants, and the Milky Way’s mass models are derived. With sufficiently large azimuthal coverage and dense sampling, such regions can be identified [e.g., the Perseus arm between $l = 90^\circ$ and $l = 120^\circ$, (Brand & Blitz 1993)], and discarded. However note that when streaming motions have maximal effect on the observed radial velocities, the effects on the proper motions will be minimal, and vice-versa. Thus, by combining the information from the line of sight and transverse motions, all azimuths can be properly sampled, which should lead to a significantly more accurate determination of the Milky Way’s rotation curve. One could then use the deviations from the general axisymmetric velocity field to study the non-circular motions in great detail and infer the mass associated with the spiral arms.

We have seen that the distribution of the ISM has a large effect on the determination of the Oort constants in the Solar neighbourhood. However, the non-circular streaming motions have not been mapped out within one kpc from the Sun because random motions dominate the radial velocity and proper motion measurements of individual tracer objects. Although Hanson (1987) overcame this problem by using over 60,000 stars in his determination of the Oort constants, his data set cannot be used to investigate non-circular motions in the Solar neighbourhood as no distances to individual objects are available for this survey.

We should keep in mind that if streaming motions are present to a significant degree, the stellar orbits will become more complex, and so the Oort constraints derived from simple stellar kinematic measurements will also be compromised. Clearly, in order to allow for these phenomena fully, one must compare a complete dynamical model for the Milky Way to the observational data. However, application of Occam’s razor to this problem suggests that the first step should be the comparison of observations to the simpler azimuthally-symmetric model. The fact that we can satisfactorily describe the Oort constraints with this model implies that there is no direct evidence for non-circular motions in Hanson’s Solar neighbourhood data. If, however, future observations establish that the true values for the Galactic constants lie outside the acceptable region in Figure 4, then at least one of the assumptions underlying our models must be wrong. For example, it might be that significant non-circular stellar motions are present. Alternatively, the mass distributions of the stars, or indeed the dark matter may be non-smooth and contribute significantly to local gradients in the rotation curve.

6 SUMMARY

We have used distance and radial velocity data available in the literature to investigate the rotation curve of the Milky Way. The accepted uncertainties in the Galactic constants of $\sim 10\%$ allow for a wide range in rotation curve shapes. We have fitted mass models to about 450 rotation curves which are consistent with the radial velocity data and determined

the Oort functions $A(R)$ and $B(R)$ for these model rotation curves. Typically, the Oort functions vary at a rate of a few $\text{km s}^{-1}\text{kpc}^{-2}$. In several locations in the Milky Way, the more objective model rotation curves show sufficient fine structure to affect the Oort functions significantly. The ring of H I just beyond the Solar circle is massive enough to flatten $A(R)$ and $B(R)$ in the first kiloparsec beyond the Solar circle. Comparison between the model $A(R)$ and $B(R)$ functions and Hanson’s (1987) determinations of the Oort constants places tight limits on the distance to the Galactic center and the Milky Way’s rotation speed at the position of the Sun: $R_0 = 7.1 \pm 0.4$ kpc, and $\Theta_0 = 184 \pm 8$ km s^{-1} . These results are consistent with the only direct determination of the distance to the Galactic center, $R_0 = 7.2 \pm 0.7$ kpc, by Reid (1993), and the proper motion of Sgr A* (Backer & Sramek 1987; Backer 1996; Reid 1998). With these Galactic constants we find that the rotation curve of the Milky Way declines slowly in the outer Galaxy. At larger distances from the Sun these models are entirely consistent with recent determinations of the Oort constants based on radial velocities and proper motions of Cepheids.

ACKNOWLEDGEMENTS

We thank Andy Newsam for useful discussions. We also thank the referee, Gerry Gilmore, for providing valuable suggestions, which have greatly improved the manuscript. MRM is supported by a PPARC Advanced Fellowship (B/94/AF/1840).

REFERENCES

- Alcock C. et al. , 1995, *ApJ*, 449, 28
 Backer D.C., 1996, in Blitz L., Teuben P., eds, *Unsolved Problems of the Milky Way*
 Backer D.C., Sramek R.A., 1987, in Backer D.L., eds, *AIP Conf. Proc. AIP*, New York, p. 163
 Bahcall J.N., Schmidt M., Soneira R.M., 1983, *ApJ*, 265, 730
 Becquaert J.F., Combes F., Viallefond F., 1997, *A&A*, 325, 41
 Begeman K., 1989, *A&A*, 223, 47
 Begeman K., 1987, Ph. D. Thesis, University of Groningen
 Binney J.J., Dehnen W., Houk N., Murray C.A., Penston M.J., 1997, to appear in the ‘‘Proceedings of the Hipparcos, Venice 1997 Symposium’’, Published by ESA as ESA-SP 402, RGO preprint No. 272
 Brinks E., Burton W.B., 1984, *A&A*, 141, 195
 Broeils A.H., 1992, Ph. D. Thesis, University of Groningen
 Broeils A.H., 1992b, *A&A*, 256, 19
 Brand J., Blitz L., 1993, *A&A*, 275, 67
 Bronfman L., Cohen R.S., Alvarez H., May J., Taddeus P., 1988, *ApJ*, 324, 248
 Burton W.B., 1988, in Verschuur G.L., Kellermann K.I., eds, *Galactic and Extragalactic Radio Astronomy*, p. 295
 Caldwell J.A.R., Ostriker J.P., 1982, *ApJ*, 251, 61
 Casertano S., van Gorkom J.H., 1991, *AJ*, 101, 1231
 Crampton D., Bernard D., Harris B.L., Thackeray A.D., 1976, *MNRAS*, 176, 683
 Dehnen W., Binney J.J., 1997, submitted to *MNRAS*, astro-ph, 9612059
 Delhaye J., 1965, in Blaauw A., Schmidt M., eds., *Stars and Stellar Systems*, Vol. 5., p. 61 (D65)
 Deul E. R., van der Hulst J.M., 1987, *A&AS*, 67, 509
 Evans N.W., Jijina J., 1994, *MNRAS*, 267, L21

- Feast M., Whitelock P., 1997, MNRAS, in press (astro-ph/9706293)
- Fich M., Tremaine S., 1991, ARA&A, 29, 409
- Gates E.I., Gyuk G., Turner M.S., 1995, PhRvL, 74, 3724
- Gould A., Ramirez S.V., 1997, astro-ph/9705174
- Hanson R.B., 1987, AJ, 94, 409 (H87)
- Kent S.M., 1992, ApJ, 387, 181
- Kent S.M., 1989, AJ, 97, 1614
- Kent S.M., 1987, AJ, 93, 816
- Kerr F.J., Lynden-Bell D., 1986, MNRAS, 221, 1023 (KLB86)
- Klemola A.R., Jones B.F., Hanson R.H., 1987, AJ, 94, 501
- Kuijken K., Gilmore G., 1989, MNRAS, 239, 605
- Kuijken K., Tremaine S., 1994, ApJ, 421, 178
- Lake G., Feinswog L., 1989, AJ, 98, 166
- Malhotra S., 1995, ApJ, 448, 138
- McCuskey S.W., 1965, in Blaauw A., Schmidt M., eds., Stars and Stellar Systems, Vol. 5., p. 15
- Mayor M., 1974, A&A, 32, 321
- Metzger, M.R., Caldwell, J.A.R., Schechter, P.L., 1998, astro-ph, 9710055
- Mihalas D., Binney J., 1981, Galactic Astronomy, Freeman, San Francisco
- Merrifield M.R., 1992, AJ, 103, 1552
- Oblak E., 1983, A&A, 123, 238
- Olive K.A., Steigman G., 1995, ApJS, 97, 490
- Olling R.P., 1996a, AJ, 112, 457
- Olling R.P., 1995, AJ, 110, 591
- Olling R.P., Merrifield M.R., 1998a, in final stage of preparation
- Oort J.H., 1965, in Blaauw A., Schmidt M., eds., Stars and Stellar Systems, Vol. 5., p. 455
- Persic M., Salucci P., Stel F., 1996, MNRAS, 281, 27
- Pont F., Mayor M., Burki G. 1994, A&A, 285, 415
- Reid I.N., Hawley S.L., Gizis J.E., 1995, AJ, 110, 1838
- Reid M.J., 1998, BAAS, 29, #97.06
- Reid M.J., 1993, ARA&A, 31, 345
- Reid M.J., 1989, in Morris M., eds, The Center of the Galaxy, IAU 136, Dordrecht, Kluwer, p. 37
- Rohlfs K., Kreitschmann, J., 1988, A&A, 201, 51
- Rubin V.C., Burstein D., Ford W.K., Thonnard N., 1985, ApJ, 289, 81
- Sackett P.D., 1997, ApJ, 483, 103
- van Albada T.S., Sancisi R., 1986, Phil. Trans. R. Soc. Lond. A., 320, 447
- Vyssotsky A.N., Janssen E.N., 1951, AJ, 56, 58
- Wouterloot J.G.A., Brand J., Burton W.B., Kwee K.K., 1990, A&A, 230, 21